OPTIMIZED AEROSOL JET PRINTED SILVER CONTACTS ON LOWLY DOPED PHOSPHORUS AND BORON EMITTERS

Sebastian Binder, Christian Schmiga, Markus Glatthaar and Stefan W. Glunz

Fraunhofer Institute for Solar Energy Systems (ISE)
Heidenhofstr. 2, D-79110 Freiburg, Germany
Phone: +49-761 4588 5938 Fax: +49-761 4588 9250 E-Mail: Sebastian.Binder@ise.fraunhofer.de

ABSTRACT: For highly efficient silicon solar cells, lowly doped phosphorus or boron emitters are essential prerequisites to achieve sufficient surface passivation. However, contact formation to such lowly doped surfaces remains a challenge for traditional printing technologies. The question arises if such emitters can be contacted reliably applying advanced metallization inks. For this investigation, we manufactured lowly doped boron and phosphorus emitters with $N_{D/A} < 1 \cdot 10^{20}$ cm^{-3} onto silicon substrates with high pyramid texture. For metallization we used our optimized aerosol jet printing process and altered the ink deposition density from 6 to 23 g/m². On textured wafers the seed layer width remained < 40 µm in average with our own developed seed layer ink. For characterization purposes the lines were thickened with electro-plated silver. Contact resistivity measurements were performed to judge the suitability of this metallization scheme. It is shown that contact formation mainly depends on the firing temperature and less on the amount of deposited ink. Contact resistivities of 1-7 mΩ·cm² for the phosphorus and 6-12 mΩ·cm² for the boron emitter could be achieved.
Keywords: Metallization, Contact Resistance, Fine-line Printing, Aerosol Jet Printing

1 INTRODUCTION

Printing and firing of silver inks or pastes is the preferred way to form contact to the front emitter during silicon solar cell fabrication in common PV production lines. To further improve the cell efficiencies, lowly doped phosphorus or boron emitters are becoming more important. For high-potential solar cell concepts, the peak doping concentration $N_{D/A}$ at the surface of the emitter, however, is much lower than for standard cell concepts [1] and reaches doping concentrations below $1 \cdot 10^{20}$ cm^{-3} [2, 3]. To enable practical industrial high throughput production at low costs, these emitters need to be contacted by printing technologies. It has already been shown that a seed layer silver ink deposited by aerosol jet printing forms good electrical contact to emitters featuring even very low phosphorus doping concentrations of $N_D = 8 \cdot 10^{18}$ cm^{-3} [4].

In this study, we have further improved our aerosol jet printing process to allow for the deposition of lines with high aspect ratio and reduced number of scattered droplets. The fabricated samples were fired at different peak temperatures and thickened by electrochemical deposition of silver [5]. The geometry of the printed contact lines, the ink deposition density and resulting contact resistances on lowly doped phosphorus and boron emitters with $N_A = 1 \cdot 10^{20}$ cm^{-3} and $N_D = 8 \cdot 10^{19}$ cm^{-3}, respectively, as used for highly efficient solar cells are discussed.

2 TEST SAMPLE STRUCTURE

For our investigation, two groups of symmetric test samples (n^+pn^+ and p^+np^+) were fabricated on 100 mm float-zone (FZ) silicon wafers with a base resistivity of 1 Ohm·cm (see figure 1). Figure 2 provides an overview of the process flow for this investigation.

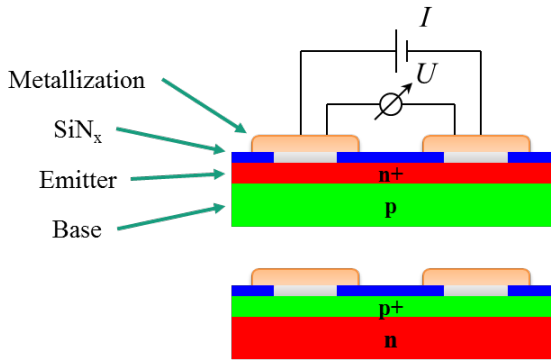

Figure 1: Symmetric test sample structures (surface texture omitted for clarity).

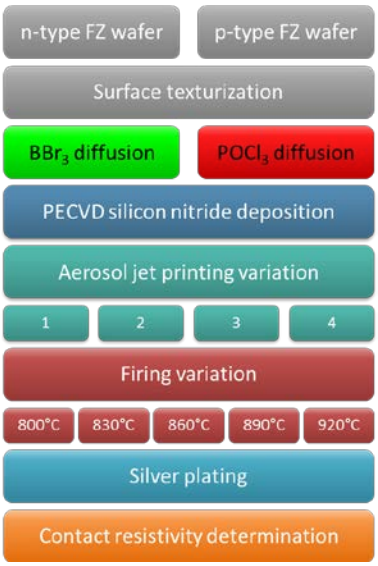

Figure 2: Process flow for this investigation.

After cleaning the surface of the bare wafers, a small group was put aside and its surface been chemically polished. This group was used as reference for the

diffusion and printing processes. The surfaces of the other wafers were chemically textured in KOH solution to produce randomly distributed pyramids. The produced pyramids were analyzed by laser-confocal imaging. An algorithm was used to detect the pyramid tips and calculate the size distribution within 116x87 µm areas. The mean height of the pyramids was h = 10.0 µm (figure 3), the root mean square (RMS) surface roughness was determined with SRq = 2.3 µm with a maximum height of roughness of SRz = 14.5 µm. For printing narrow structures such a rough surface is challenging. When the liquid ink is transferred to the surface it tends to flow into the trenches and wet the surface. The higher the pyramids, the wider the valleys in between and the further the ink may creep or droplets are deflected. Smaller pyramids are favorable for printing.

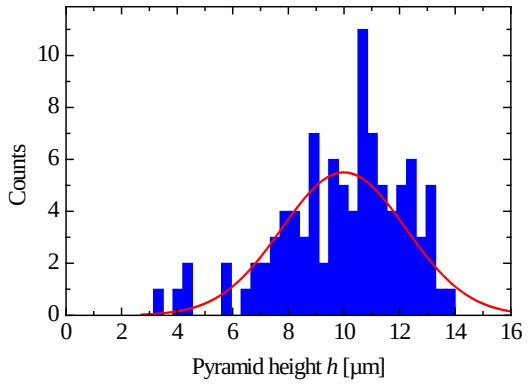

Figure 3: Histogram of pyramid height distribution

The *p*-type test samples received a $POCl_3$-diffused emitter with a sheet resistance of about $R_{SH,D}$ = 106 Ohm and a phosphorus peak doping concentration at the surface of $N_D = 8 \cdot 10^{19}$ cm^{-3}. The *n*-type wafers with BBr_3-diffused emitter featuring a sheet resistance of about $R_{SH,A}$ = 90 Ohm and a peak doping concentration of $N_A = 1 \cdot 10^{20}$ cm^{-3} were fabricated. The emitter profiles were verified via electrochemical capacitivity voltage (ECV) measurements on the planar reference wafers. The profiles are shown in figure 4. To determine the sheet resistance of these emitters, the charge carrier mobility was calculated according to the empirical findings of *Klaassen* and integrated over the depth profiles [6].

Subsequently, a 75 nm thin silicon nitride anti-reflection coating (SiN_X) was deposited on both sides of the samples by means of plasma-enhanced chemical vapor deposition (PECVD).

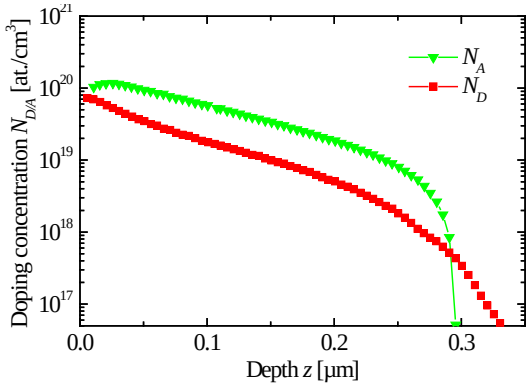

Figure 4: ECV profiles of the two emitters.

A seed layer silver ink developed at Fraunhofer ISE was used for the aerosol jet printing process. The ink is optimized for seed layer contact formation to the emitter. Four different groups were processed to alter the finger geometry and the ink deposition density ρ_{dep}: For group 1 the ink deposition density was the same as for group 2 but the line width was decreased to 28 µm. For group 2 to 4 the ink deposition density was constantly increased from 5.9 to 22.6 g/m² by multiple overprint. This increase also resulted in a small increase of line width.

For further processing, the wafers were cut into four pieces to increase the number of samples and to improve statistics. Contact firing of the samples was applied in a conveyor belt firing furnace. The samples were fired at five different set peak temperatures varying from 800 to 920 °C in steps of 30 K. Being able to perform electrical measurements, subsequently, the seed layers were thickened by electro-plating of silver. Therefore the busbars were contacted with the electrode and about 12 mg of silver per sample were deposited. For contact resistance measurement (TLM), stripes with a width of 5 mm were cut out using a dicing saw. The contact resistances were determined with the transfer-length measurement system from KB·ESI.

3 CONTACT RESISTANCE MEASUREMENTS

To determine the contact resistivity according to the transfer-length method (TLM), two different measurement procedures need to be performed: *(i)* contact resistance measurements to receive the contact resistance R_C and the sheet resistance R_{SH}, *(ii)* end of line resistance measurements to gain the transfer-length and, subsequently, the specific contact resistivity ρ_C.

The contact resistance measurement (*i*) is performed for different finger distances. The data is plotted and linearly fitted. Its y-axis cross section equates $2 \cdot R_C$ and its slope corresponds to the sheet resistance R_{SH}. The coefficient of determination R^2 of this fit is a measure of quality for this measurement. Figure 5 sketches the measurement setup. The whole measurement theory is described by *Schroder* [7].

Important boundary conditions to this technique are the assumption that all fingers are identical. With printed and fired contacts this is barely achieved, because contact sintering happens locally underneath the finger area. Generated silver crystallites or tunneling contacts is distributed randomly [8]. This leads to an increase of measurement uncertainty compared to evaporated and annealed contacts, e.g. titanium-palladium-silver. The geometry of the sample must also be well defined to have the applied current being well distributed. Therefore a 5-10 mm wide stripe needs to be cut out orthogonally to the fingers before measurement.

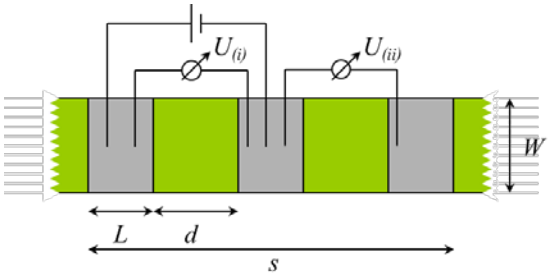

Figure 5: Setup for contact resistivity measurements.

4 OPTIMIZED AEROSOL JET PRINTING

Aerosol jet printing is a direct-write printing technology by which an ink is atomized pneumatically with a Venturi nozzle. However, the generated aerosol is very dilute. With the use of a virtual impactor excess carrier gas is sucked off the system and the aerosol droplet volume fraction increased. This aerosol flow is guided into a print head where it is aerodynamically focused by a sheath gas and guided through nozzles (see figure 6). In these experiments the nozzles have an inner diameter of d_n = 0.15 mm; a print head with a ten nozzle array was used for printing.

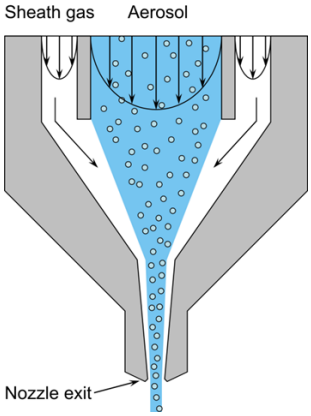

Figure 6: Sketch of a single nozzle aerosol jet print head demonstrating focusing of the aerosol flow.

The fluid flow in the print head can be controlled by adjusting the sheath-gas to aerosol-flow ratio. This ratio must fit to the desired printed structure and the print head design. With adjusting this ratio, the aerosol droplet trajectories and the mass throughput can be controlled and a narrow aerosol jet can be generated [9].

For printing, the substrate is placed about 2-3 mm below the exit of the printing nozzle. To enable sharp-defined and narrow lines, in addition to the optimization of the aerosol jet, the substrate needs to be heated to evaporate deposited solvents and to prevent wetting of the ink within the pyramidal valleys. The wafers were heated to T = 150 °C. The ink used for seed layer formation is based on the results of Hörteis et al., Binder et al. and Kalio et al. [4,8,10]. It is optimized for contact formation to lowly doped surfaces. The ink consists of silver powder, glass frit and metal oxides – all in a specific size distribution dispersed in an organic vehicle system with low viscosity to improve atomization.

With this technology, narrow line widths can be achieved. Advantages of this process are the contactless deposition of conductive lines, the possibility to regulate and control the printed line widths and the possibility to easily test new materials and ink compositions. Furthermore with this seed and plate concept independent optimization of the metal-semiconductor contact and the lateral line conductivity is possible.

5 CHARACTERISTICS OF THE PRINTED LINES

Reference lines were printed onto planar wafers with the optimized aerosol jet process. The planar surface offers the advantage that wetting effects such as bleeding are minimized. Line widths of less than 17 µm in average were printed – demonstrating the potential of the aerosol jet printing process. The line widths achieved on the planar surface are compared to the line widths on wafers with large randomly distributed pyramids (see figure 7). Due to surface wetting, capillary effects and the momentum of the impacting droplets the printed lines on the pyramidal surface are about 30 - 40 % wider than on the planar surface. So the minimum achievable line width is not only depending on the process but also on the morphology of the substrate. With a laser confocal microscope the mean cross-section of the lines printed on the planar reference wafers was determined. The height of the lines printed on the textured wafers was then calculated by dividing the corresponding cross-section by the measured line widths. The so obtained finger height equals a rectangular cross-section height and was in the range of about 1 to 5 µm. Table I provides an overview of the averaged line characteristics for each group.

For group 1 and 2 the deposition density ρ_{dep} was kept constant (ρ_{dep} = 5.9 g/m²). It was increased for the other groups (figure 8). The variation in deposited amount of ink equals to a variation of the glass frit content deposited onto the surface. This different source of etchants may also influence contact formation of the different groups.

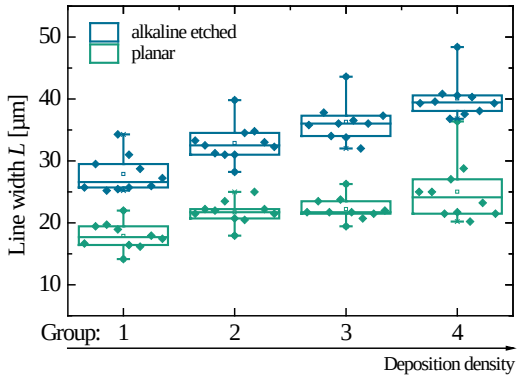

Figure 7: Line widths on planar (bottom) and pyramidal textured (top) surface.

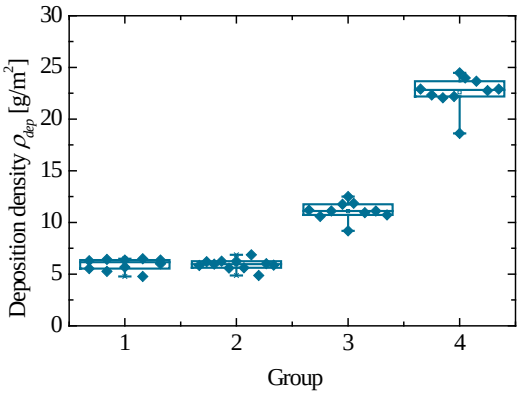

Figure 8: Aerosol jet printed deposition densities on the alkaline textured wafers for the different groups.

Table I: Average geometric line data for textured wafers.

Group	*1*	*2*	*3*	*4*
Deposition density ρ_{dep} [g/m²]	5.9	5.9	11.1	22.6
Line width L [µm]	27.9	33.1	36.3	40.1
Finger height h [µm]	1.5	1.4	2.7	4.7
Aspect ratio	0.05	0.04	0.07	0.12

6 ELECTRICAL CONTACT PROPERTIES

The variation of the printing and firing conditions influences the contact formation mechanisms on these two emitters. If any of the process steps were not homogeneous, the contact would also not be homogeneously sintered and contact resistance determination can become difficult. To evaluate what contact resistance measurement results were reasonable, they were first sorted by their coefficient of determination R^2, which is a measure of the quality of the contact resistance measurement. It can be seen that for both emitters a reliable contact formation becomes more likely with increase of the firing temperature (see figures 9). At higher firing temperatures, the deviation of R^2 decreases clearly and approaches unity. For further analysis, only results with a coefficient of determination $R^2 > 0.98$ are considered.

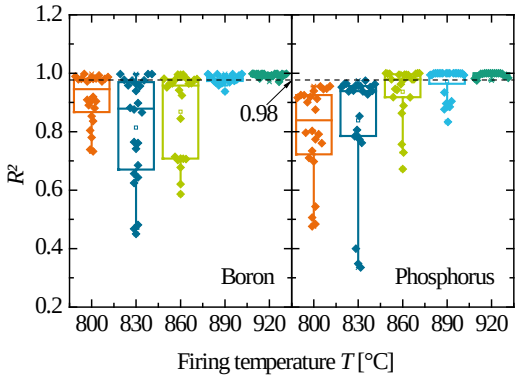

Figure 9: Coefficient of determination of the linear fits in transfer-length measurement, independently of the printing variation.

While with higher firing temperatures, contact formation becomes more reliable, the contact resistivity ρ_C also improves steadily (see figure 10). This trend is independent on the amount of printed ink. However, it may be said that under our process conditions it seems to be easier to form good contact to the phosphorus emitter than to the boron one. Nevertheless, the data for the phosphorus emitter obviously scatters more, which indicates a less homogeneous contact formation. For both emitters optimum contact firing temperature may not yet be reached in this experiment.

To investigate the influence of the aerosol jet printing variation on the contact formation, the contact resistivities for the three highest firing temperatures are shown for the four printing groups in figure 11: Left column for the boron and right column for the phosphorus emitter. Each group corresponds to a certain ink deposition density as presented in table I.

For the boron emitter within one temperature setting, there is no strong influence of the deposition density on the contact formation visible. A trend cannot be seen. Comparing the resistivities for boron gained at different firing temperatures, contact resistivity is decreasing by a factor of about ten from 860 to 920 °C.

Smaller contact resistivities were achieved for the phosphorus emitter. Comparing the different temperature variations with each other, it can be said that the contact resistivity decreases with higher firing temperature. Yet, to the phosphorus emitter small contact resistivities could already be achieved at lower firing temperatures than to the boron emitter. For the phosphorus emitter, there seems to be a relation between deposition density and the contact resistivity. With an increased deposition density contact resistivity may be also increased. At certain firing conditions this behavior becomes less intense. At a peak firing temperature of 920 °C this trends seem to be reversed.

Table II summarizes the averaged values of specific contact resistivity achieved for these temperatures for both emitters.

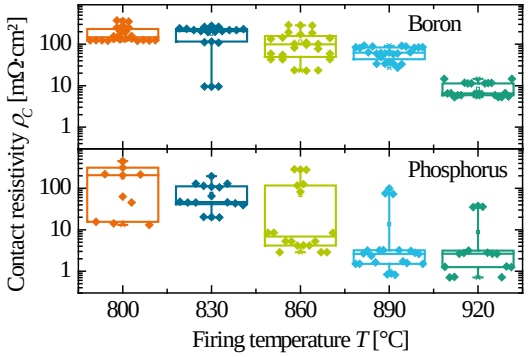

Figure 10: Reduction of specific contact resistivity for both emitters including all printing groups.

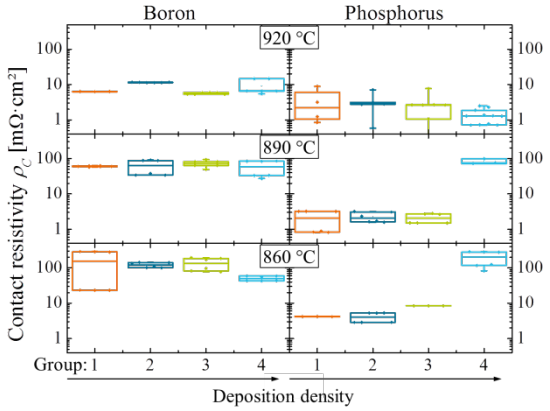

Figure 11: Contact resistivities ρ_C for the three highest firing temperatures broken down to the printing variation

Table II: Contact resistivities ρ_C achieved for the boron and phosphorus emitters.

Firing temperature	*Emitter doping* *Boron*	*Phosphorus*
860 °C	~22-150 mΩ·cm²	~4 mΩ·cm²
890 °C	~60-70 mΩ·cm²	~2-3 mΩ·cm²
920 °C	~6-12 mΩ·cm²	~1-7 mΩ·cm²

7 SUMMARY

In this experiment the authors were able to successfully contact lowly doped n^+ and p^+ emitters of silicon solar cells with $N_{D/A} < 1 \cdot 10^{20}$ cm^{-3} using a two-layer metallization technique with optimized aerosol jet printing and subsequent plating of silver. Narrow seed layers were fabricated with variation in deposition density and finger height. The line width was varied between 28 and 40 µm on a large randomly textured surface. With the same optimized printing process, line widths down to 17 µm in average are achieved on planar reference wafers, demonstrating the potential of printing narrow structures with this technology. The ink deposition density was altered between 6 and 23 g/m². The samples were fired at five different temperatures and contact formation was investigated by measuring contact resistivities with the transfer-length method (TLM).

It is observed that the firing temperature is the most critical parameter for contact formation. The dependency on the deposition density is less critical for seed layer contact formation. Forming good contact to the n^+ region already occurs at lower temperatures than to the p^+ region. Contact resistivities of 1-7 mΩ·cm² for the phosphorus emitter and 6-12 mΩ·cm² for the boron emitter are achieved.

With this investigation we have shown that it is possible to contact both lowly doped n^+ and p^+ surfaces of silicon solar cells satisfyingly using aerosol jet printed seed layers.

ACKNOWLEDGEMENT

The authors gratefully acknowledge the contribution of other members of Fraunhofer ISE, F. Schätzle and A. Tuschinsky for sample preparation in the clean room, K. Krüger for ink preparation, A. Khanna for discussions on surface texture and M. Wichmann for electrical characterization.

REFERENCES

[1] Benick, J., et al., Applied Physics Letters, 2008. **92**(253504): p. 253504/1-3.
[2] Hermle, M., Faculty of Physics, 2008, University of Constance, p. 198.
[3] Reichel, C., et al., Progress in Photovoltaics: Research and Applications, 2013. **21**(5): p. 1063-1076.
[4] Binder, S., et al., Energy Procedia, 2012. **21**: p. 32-38.
[5] Bartsch, J., et al., Proceedings of the 27th European Photovoltaic Solar Energy Conference and Exhibition. 2012. Frankfurt, Germany.
[6] Klaassen, D. B. M., 1992. Solid-State Electronics **35**(7): 953-959.
[7] Schroder, D. K., 2006. Semiconductor material and device characterization. Hoboken, New Jersey, USA, John Wiley & Sons.
[8] Hörteis, M., et al., Advanced Functional Materials, 2010. **40**: p. 476-484.
[9] Binder, S., et al. Aerosol Science and Technology, 2014, **48**(9): p. 924-929.
[10] Kalio, A., et al., Energy Procedia, 2013. **38**(0): p. 745-752.